Supporting Information

Copper depletion-induced tumor cuproptosis

Min Zhou,[1#] Faheem Muhammad,[1#,5] Yihong Zhang,[1] Tong Li,[1] Jiayuan Feng,[1,4] Jingyuan Zhao,[1] Hui Wei[1,2,3]*

[1]Department of Biomedical Engineering, College of Engineering and Applied Sciences, Nanjing National Laboratory of Microstructures, Jiangsu Key Laboratory of Artificial Functional Materials, Nanjing University, Nanjing, Jiangsu 210023, China.

[2]State Key Laboratory of Analytical Chemistry for Life Science, School of Chemistry and Chemical Engineering, Chemistry and Biomedicine Innovation Center (ChemBIC), ChemBioMed Interdisciplinary Research Centre at Nanjing University, Nanjing University, Nanjing, Jiangsu 210023, China.

[3]Nanozyme Laboratory in Zhongyuan, Henan Academy of Innovations in Medical Science, Zhengzhou, Henan 451163, China.

[4]Department of Materials Engineering, Graduate School of Engineering, The University of Tokyo, Tokyo 113-8656, Japan.

[5]Guangdong Key Laboratory of Biomedical Measurements and Ultrasound Imaging, School of Biomedical Engineering, Shenzhen University Medical School, Shenzhen University, Shenzhen, Guangdong 518000, China.

#Equal contribution.

*Corresponding authors.

E-mail: weihui@nju.edu.cn.

Keywords: Copper homeostasis, Cuproptosis, Copper depletion, Anti-tumor ability, Mechanism of copper depletion

Table of Contents

References

Materials and Methods

Reagents

Zinc nitrate hexahydrate ($Zn(NO_3)_2 \cdot 6H_2O$), citric acid monohydrate (CA), and ethanol were obtained from Sinopharm Chemical Reagent Co., Ltd. (Shanghai, China). Cetyltrimethylammonium bromide (CTAB), thioacetamide (TAA), hexamethylene tetramine (HMTA), and dopamine hydrochloride (DA) were purchased from Sigma-Aldrich Co., Ltd. (Shanghai, China). Glut 1 DNAzyme was synthesized by Sangon Co., Ltd. (Shanghai, China), and the sequence information was shown in Table S3. Cell culture reagents (such as fetal bovine serum) were from Excel Co., Ltd. (Xian, China), HyClone™ DMEM was from Cytiva Co., Ltd. (Shanghai, China), and trypsin, penicillin-streptomycin and 2',7'-dichlorodihydrofluorescein diacetate (DCFH-DA) were from Beyotime Co., Ltd. (Shanghai, China). The antibodies for western blotting (Glut1 and β-actin antibodies) were from Bioss Co., Ltd. (Beijing, China), and the antibodies for immunofluorescence were from Huabio Co., Ltd. (Hangzhou, China). Superoxide dismutase (SOD) and the GSH/GSSH detection kits were obtained from Beyotime Co., Ltd. (Shanghai, China). The CCK-8 kit, SOD detection kit, glucose detection kit, and lactate detection kit were from Dojindo Co., Ltd. (Shanghai, China). Seahorse XF cellular mitochondrial stress test kit (No. 103015-100) and Seahorse XF glycolysis stress test kit (No. 103020-100) were from Agilent. Deionized water (18.2 MΩ·cm, Millipore) was used for material synthesis and cell culture. All these reagents were used without any further treatment.

Instrumentation

The morphology of nanoparticles was obtained by transmission electron microscopes (TEM, FEI TECNAI 12, 120 kV and FEI TECNAI G2 F30S-Twin). Powder X-ray diffraction (XRD) patterns were obtained by using a diffractometer (Bruker-AXS, Germany). X-ray photoelectron spectroscopic (XPS) analysis was carried out by a Thermo Scientific K-Alpha spectrometer (Al Kα (1486 eV)), and the related software was used for data analysis. An IR thermographic camera was from FOTRIC Co., Ltd. (Suzhou, China). Seahorse XFe96 Analyzer for cell metabolic analysis was from Agilent (USA). Inductively coupled plasma spectrometry was performed on an Agilent

5110 instrument.

Synthesis of ZnS

ZnS was prepared by ligand-assisted coordination assembly, using CTAB as the template, zinc nitrate as the inorganic precursor, citric acid and HMTA as the ligands, and TAA as the sulfur source. Briefly, $Zn(NO_3)_2 \cdot 6H_2O$ (138.8 mg), CTAB (85.0 mg), HMTA (35.0 mg), citric acid (25.0 mg), and TAA (20.0 mg) were mixed in 100 mL of deionized water. They were then stirred vigorously for 10 min at room temperature. Subsequently, the mixture was heated and kept in an air circulating oven at 85 °C for 5 h. Then, the colloidal precipitate was obtained by centrifugation. The precipitate was washed with ethanol/water several times and dried for later use.

Synthesis of "copper nanoconsumer"

The designed "copper nanoconsumer" (*i.e.*, ZnS@PDA/DNA) was synthesized as follows. To protect the ZnS core, a PDA shell was prepared by polymerization of dopamine hydrochloride (DA) on the surface of the core ZnS. ZnS and DA were mixed (weight ratio=1:1) in 10 mM Tris buffer (pH=8.5) at room temperature for 2 h. After the color of the reaction solution changed from ivory-white to light-black, the solution was centrifuged to obtain the precipitate (ZnS@PDA, termed ZP). Then, the precipitate was washed with deionized water several times and stored at 4 ℃ for further use. Next, the ZnS@PDA/DNA (termed ZPD) was obtained by adsorbing Glut1 DNAzyme (termed GD, sequences of GD and its substrate were listed in Table S3) on ZP. 10 nM GD was added to 50 μg/mL ZP with metal ions (pH=7.6, 10 mM HEPES buffer). After 1 h of incubation, the precipitate was collected and washed for later use. GD absorption kinetics were determined by adsorbing Cy3-labeled GD with ZP, and the procedures were the same as those used for GD.

Cation exchange of ZnS by Cu^{2+}

$CuCl_2$ was chosen as the donor of Cu^{2+}. The total volume of ion exchanging solution

was set at 1 mL. Various final volumes of 1 mM Cu^{2+} (0, 5, 10, 20, 30, 40, 50, and 100 μL) were added to the solution at room temperature while keeping the final concentration of ZnS at 20 μg/mL. The solution underwent a rapid reaction, resulting in a color change to yellow in seconds, and then the solution was allowed to stand for an additional 30 min to complete cation exchange reaction. Finally, the precipitated product was collected for metal content measurement by using inductively coupled plasma-optical emission spectrometry (ICP-OES).

ZPD photothermal effect analysis

Based on the photothermal effect of CuS, photothermal imaging was performed by a FOTRIC IR camera. In a typical test, 10 μg/mL materials were irradiated by an 808 nm laser with the power of 2 W/cm^2, and the temperature change was recorded at each time point (0, 1, 2, 3, 4, and 5 min). The data were analyzed with AnalyzIR and Origin.

Evaluation of ZPD properties at the cellular level

Mouse breast cancer cell line 4T1, human breast cancer cell line MCF7, mouse melanoma cell line B16, mouse colon tumor cell line CT26, and human liver cell line L02 were from ATCC. Cells were refreshed and cultured with high glucose-DMEM plus 10% FBS at 37 °C in a 5% CO_2 incubator. For cell toxicity analysis, cells were subcultured into plates with an 8×10^3 seeding density overnight. Then, cells were refreshed with the culture medium and incubated with different concentrations of ZPD for 24 h. Later, cell viability was estimated by CCK-8 kits. For copper uptake ability, cells were subcultured into 6-well plates overnight and then refreshed using culture medium with/without Cu^{2+} for next 24 h, 48 h and 72 h, respectively. Later, the cells were harvested in groups for copper content measurement by ICP-OES. Intercellular ROS level was monitored by a flow cytometer. Cells were subcultured into 6-well plates overnight and refreshed by culture medium and different concentrations of ZPD for 24 h. Subsequently, they were incubated with ROS probes DCFH-DA, and then harvested for cytometric analysis. For SOD deactivation, cells were subcultured into 6-well plates

overnight and refreshed using culture medium and ZPD with different treatments for 24 h, then cells were harvested and lysed with a sonicator. The supernatant was collected for the SOD-like activity measurement by using an SOD detection kit (WST-8). For glutathione (GSH) detection, the cells were harvested in groups, washed with PBS, and then treated with a protein removal agent. After freezing-thawing twice, the supernatant was collected for GSH content measurement by using a GSH detection kit.

Glycolytic inhibition analysis

Based on the design, the Glut 1 DNAzyme was used to cleave the Glut 1 mRNA and induce the glycolytic inhibition. Cells were treated in groups and harvested for membrane protein extraction. Western blotting was performed for monitoring Glut 1 expression. Meanwhile, the culture supernatant was collected for the glucose consumption and lactate excretion analysis. For glucose consumption detection, the supernatant was added to 96-well plates, and then working solution (from a glucose detection kit) was added to each well. Later, the reaction solution was fully mixed and incubated at 37 °C for 30 min. Finally, absorption at 450 nm was measured by a microreader. Lactate detection was executed using the same procedures as glucose detection, using a lactate detection kit.

Metabolic analysis

For mitochondrial stress test: A Seahorse XF cellular mitochondrial stress test kit (No. 103015-100) and a Seahorse XFe96 analyzer were used. 4T1 cells were subcultured into Seahorse XF96 cell culture microplates for 12 h; then cells were washed and incubated with ZnS, ZP, and ZPD (final concentration 20 μg/mL) in the glycolysis stress test medium for 24 h; finally, oxygen consumption rate (OCR) was measured by ordered injection of 1.5 μM oligomycin, 0.5 μM carbonyl cyanide-4 (trifluoromethoxy)phenylhydrazone (FCCP), and 0.5 μM Rotenone & Antimycin A (final concentration of per well).

For glycolysis stress analysis: A Seahorse XF glycolysis stress test kit (No.

103020-100) and a Seahorse XFe96 analyzer were used. 4T1 cells were subcultured into Seahorse XF96 cell culture microplates for 12 h; then cells were washed and incubated with ZnS, ZP, and ZPD (final concentration 20 μg/mL) in the glycolysis stress test medium without glucose or pyruvate for 24 h; finally, extracellular acidification rate (ECAR) was measured by ordered injection of 10 mM glucose, 1 μM oligomycin, and 50 mM 2-deoxy-glucose (final concentration of per well).

"Copper nanoconsumer"-mediated anti-tumor ability

All animal procedures were performed in accordance with the Guidelines for Care and Use of Laboratory Animals of Nanjing University and approved by the Animal Ethics Committee of Experimental Animals Welfare and Ethics of Nanjing Drum Tower Hospital, the Affiliated Hospital of Medical School, Nanjing University (No: 2021AE01042). BLAB/c mice were chosen for the construction of the breast cancer model. Mice were purchased from Nanjing Medical University and fed in a standard specific pathogen free (SPF) environment. 4T1 cells were cultured, harvested, and then washed with PBS several times. The cell suspension was obtained and subcutaneously injected into the right flank of mice with a density of 1×10^6 cells/mouse. The volume of tumors was monitored and calculated according to the formula V = length × width × width/2 (length and width of tumor were measured by using a digital caliper). When the tumor volume reached 50 mm^3, the mice were separated into groups according to the experimental plan and treated with drugs by intravenous injection (5 mg/kg per drug per mouse). In the laser group, 12 h after the drugs were injected, the tumors were irradiated with a laser (808 nm for 5 min at 2 W/cm^2). After treatments, the mice were kept for another several days and harvested for anti-tumor analysis. Each tumor was dissected for the immunofluorescence analysis. The major organs, such as the heart, liver, spleen, lung, and kidney, were also dissected for biosafety estimation.

"Copper nanoconsumer"-mediated anti-metastasis ability

BLAB/c mice were also chosen for the construction of an anti-metastasis model. Mice

were fed in a standard SPF environment. First, a 4T1 subcutaneous tumor model was obtained using the same procedure as mentioned above. After the tumor formation, the cell suspension was intravenously injected into mice. Then, the mice were treated with drugs by intratumoral injection. The laser irradiation (808 nm for 5 min at 2 W/cm^2) was also used for the treatment. Later, the lungs were harvested for the anti-metastasis analysis. The metastatic nodules were calculated. The lungs were also analyzed using the hematoxylin and eosin (H&E) staining.

Biodistribution analysis

For biodistribution analysis, different organs (heart, liver, spleen, lung, kidney, and tumor) were collected 24 h after ZPD treatment. 500 mg of each organ was separated and digested for elemental content analysis (including copper, zinc, and sulfur) by ICP-OES. Each group was prepared for three independent samples. The content was calculated and depicted using histograms.

Immunofluorescence analysis of the dissected tumor

To explore the anti-tumor and anti-metastasis mechanisms, the dissected tumors were prepared for immunofluorescence analysis, such as glucose transporter 1 (Glut 1) expression, CRT (calreticulin) exposure, HMGB1 (high mobility group protein 1) release, and $CD8^+$ T cell infiltration. The dissected tumors were mounted by OCT compound for 5 μm slices. The slices were used for immunofluorescence analysis by standard protocols and were observed by a confocal microscope. The fluorescent intensity was analyzed by ImageJ and data were obtained by Origin.

Cytokine detection

Tumor-bearing mice were treated with drugs and laser irradiation. Later, the peripheral blood was collected and left for clotting, and then the serum was used for TNF α and IFN γ detection. The detection was carried out using the corresponding enzyme-linked immunosorbent assay (ELISA) kits. Each experiment was performed four times

independently.

Table S1. Solubility product constants of ZnS and CuS in some studies.

Year of publish	K_{sp} of ZnS	K_{sp} of CuS	References
1936	1.15×10^{-26}	3.48×10^{-38}	[1]
1952	8×10^{-25}	8×10^{-36}	[2]
1958	8.8×10^{-25}~1.1×10^{-21}	8.7×10^{-36}	[3]
2010	1.6×10^{-24}	6.3×10^{-36}	[4]
2011	1.6×10^{-24}	6.3×10^{-36}	[5]
2015	1.6×10^{-24}	6.3×10^{-36}	[6]
2020	1.6×10^{-24}	6.3×10^{-36}	[7]
2020	4.0×10^{-24}	2.0×10^{-47}	[8]
2021	3.0×10^{-25}	1.0×10^{-48}	[9]
2022	1.6×10^{-24}	1.3×10^{-36}	[10]
2022	2.2×10^{-22}	2.5×10^{-48}	[11]
2024	2.9×10^{-25}	6.3×10^{-36}	[12]

Table S2. Representative copper-based clinical/preclinical therapies.

Agent	Action	Indication and testing stage	References
Clioquinol	Ionophore	Fungal infection (approved)	[13]
CuII(atsm)	Ionophore	Amyotrophic lateral sclerosis (phase II)	[14]
Disulfiram	Ionophore	Glioblastoma (phase I/II)	[14-16]
Elesclomol	Ionophore	Melanoma (phase III)	[17]
D-penicillamine	Chelator	Wilson's disease (approved)	[18]
Tetrathiomolybdate	Chelator	Wilson's disease (phase II)	[16,19,20]
Trientine	Chelator	Wilson's disease (approved)	[18]
WTX101	Chelator	Wilson's disease (phase III)	[21]
DC_AC50	Inhibitor	Melanoma (preclinical)	[22]
PTU dendrimers	Chelation	---	[23]
CDN nanoparticles	Depleting	---	[24]
ZPD nanoparticles	Depleting	---	This study

Table S3. Sequences of DNAzyme and substrate.

Name	Sequence (5' to 3')
DNAzyme	ACCAGGGCTCCGAGCCGGTCGAAACTTCAAAGA
Substrate	TCTTTGAAGT/rA/GGCCCTGGT
Cy3-DNAzyme	Cy3-ACCAGGGCTCCGAGCCGGTCGAAACTTCAAAGA

Note: all the DNA samples were synthesized by Sangon Biotech (Shanghai) Co., Ltd.

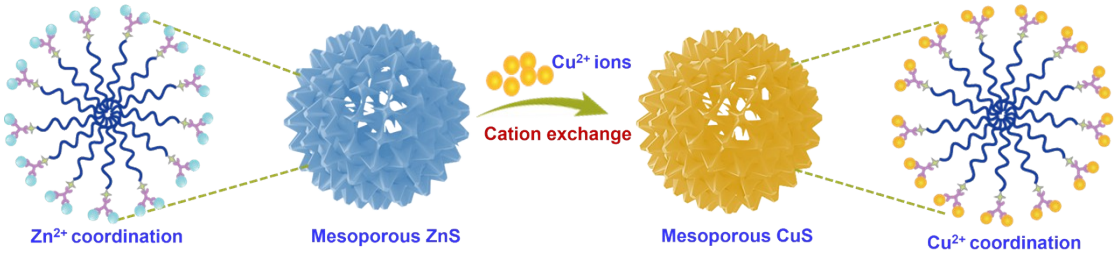

Figure S1. Scheme of cation exchange reaction between Cu^{2+} and ZnS based on the large difference of their solubility product (K_{sp}).

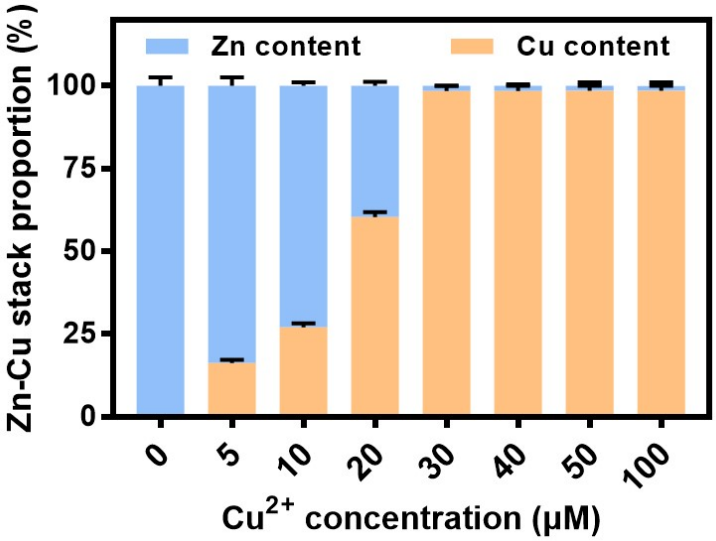

Figure S2. Zn-Cu stack proportion by adding Cu^{2+} into ZnS solution. Each error bar represents the standard deviation of four independent measurements.

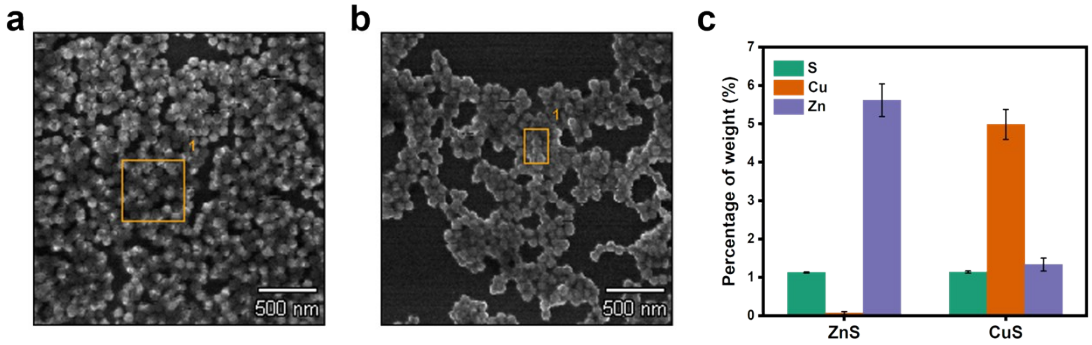

Figure S3. EDS analysis of copper and zinc contents. SEM images of ZnS (a) and ZnS after Cu chelation (b). Orange squares indicate the areas for EDS analysis. (c) Percentage of atoms in each group by normalizing to the S element. Each error bar represents the standard deviation of three independent measurements.

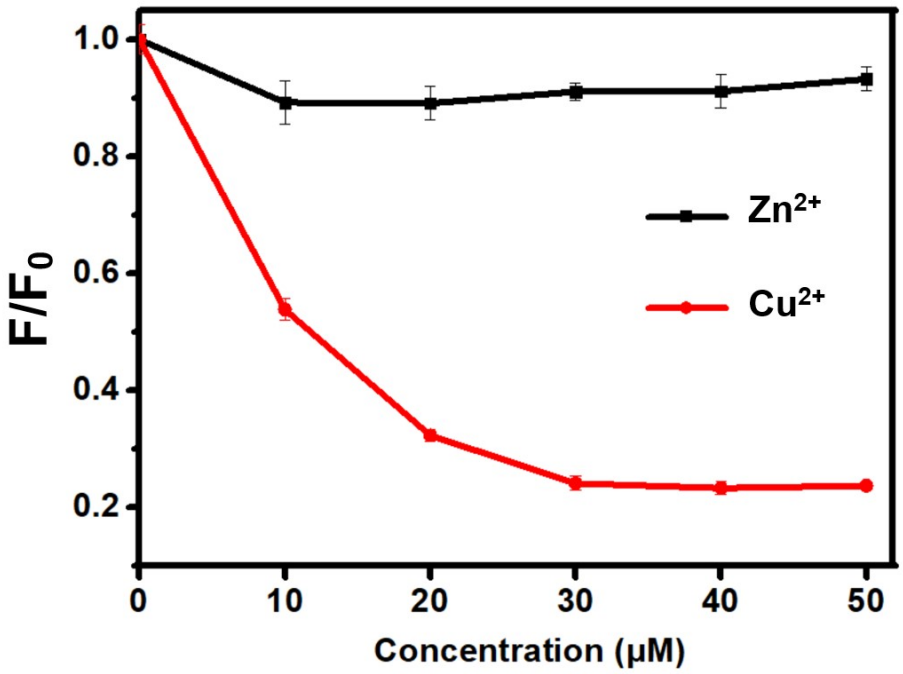

Figure S4. Metal ion-mediated fluorescence quenching of Cy3-labled GD. Each error bar represents the standard deviation of four independent measurements.

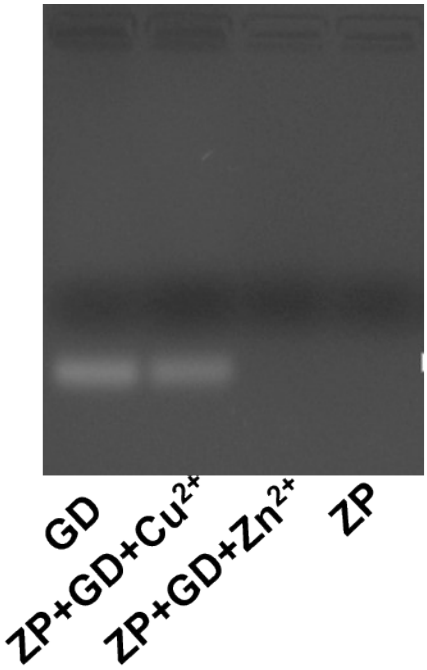

Figure S5. Gel electrophoresis analysis of the GD conjugation.

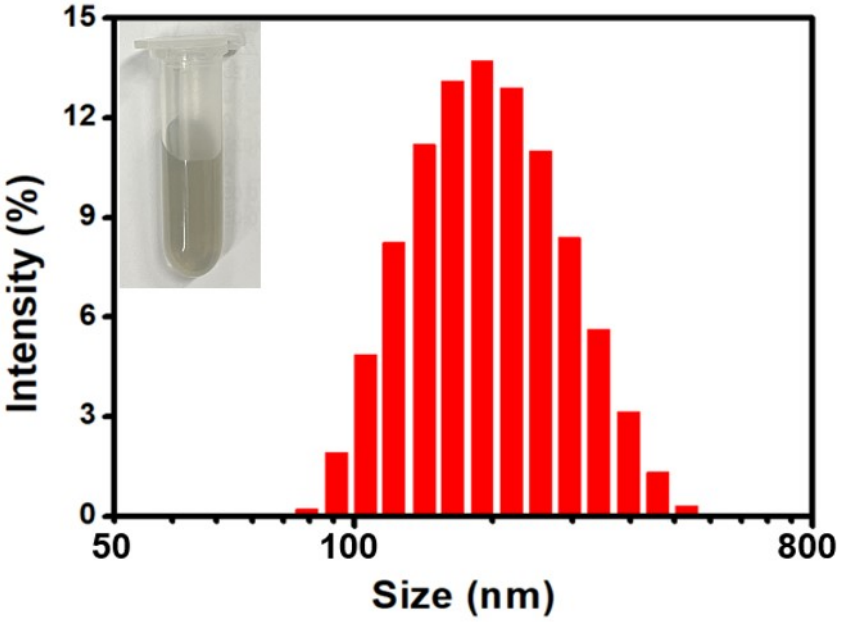

Figure S6. Size distribution histogram of ZPD. Inset: digital photo of ZPD solution.

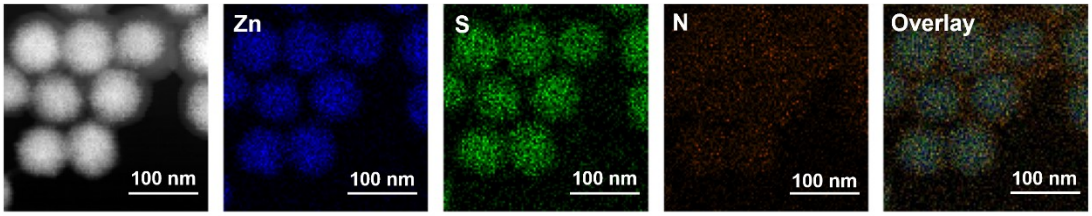

Figure S7. Elemental mapping analysis of ZPD.

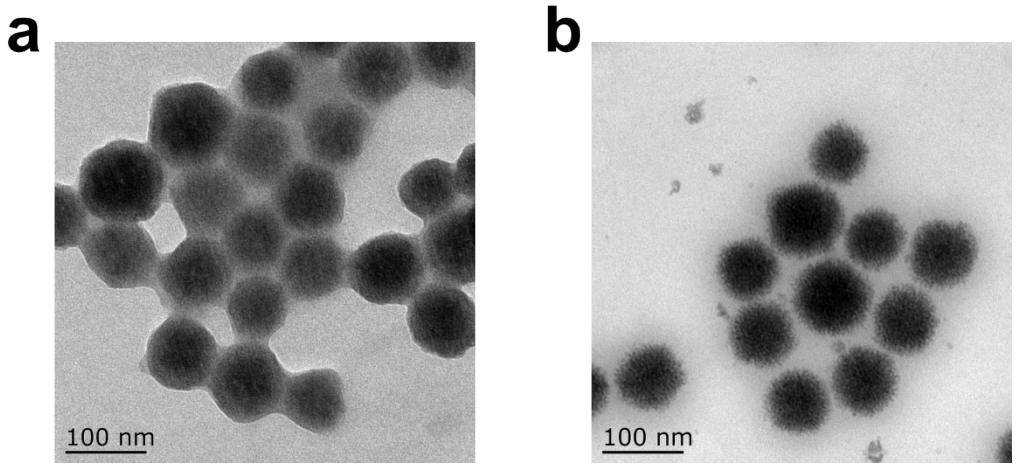

Figure S8. Acid-induced PDA-shell degradation of ZPD. TEM images of ZPD nanoparticles after treatment with acid (pH 5.8) for (a) 12 h and (b) 24 h.

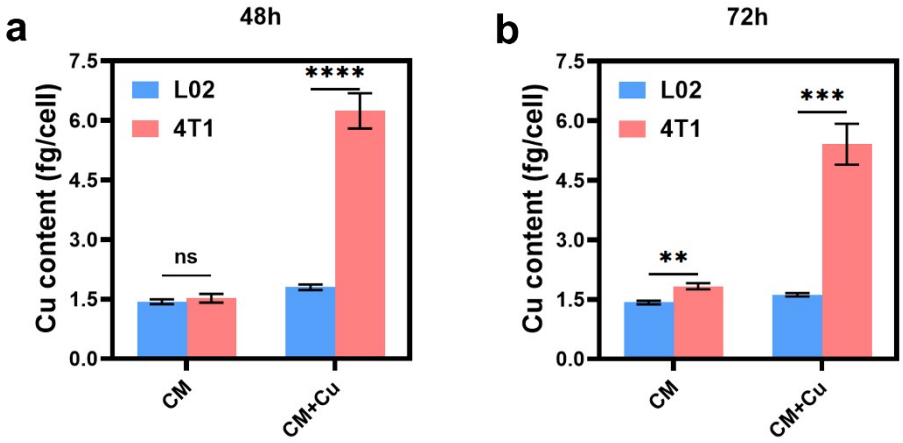

Figure S9. Cellular copper stack percentage with/without addition of Cu^{2+} to culture medium after different time point treatment (48 h and 72 h). CM: culture medium, CM+Cu: culture medium plus Cu^{2+}. Each error bar represents the standard deviation of four independent measurements. Ordinary one-way ANOVA was used for discrepancy analysis (*P<0.05, **P<0.01, ***P<0.001, ****P<0.0001).

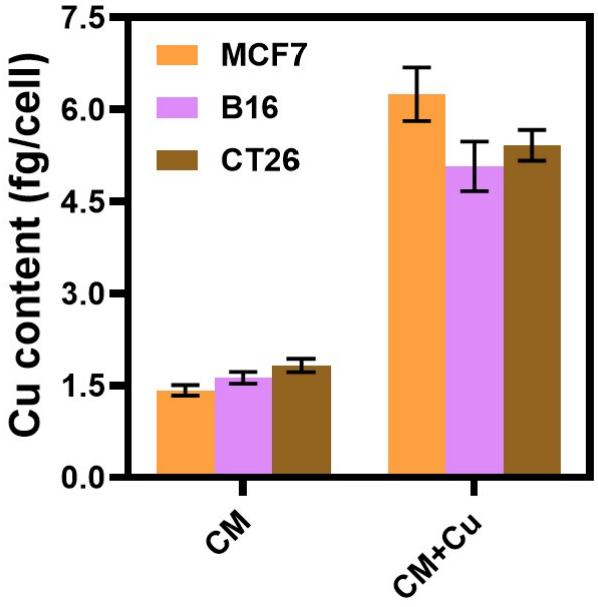

Figure S10. Cellular copper stack percentage with/without addition of Cu^{2+} to culture medium (24 h). CM: culture medium, CM+Cu: culture medium plus Cu^{2+}. Each error bar represents the standard deviation of four independent measurements.

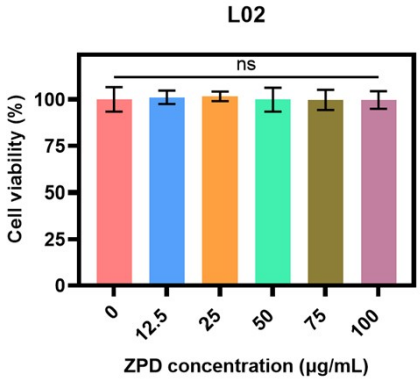

Figure S11. Cell viability analysis of ZPD at different concentrations for L02 cells. Each error bar represents the standard deviation of four independent measurements. Ordinary one-way ANOVA was used for discrepancy analysis (*P<0.05, **P<0.01, ***P<0.001, ****P<0.0001).

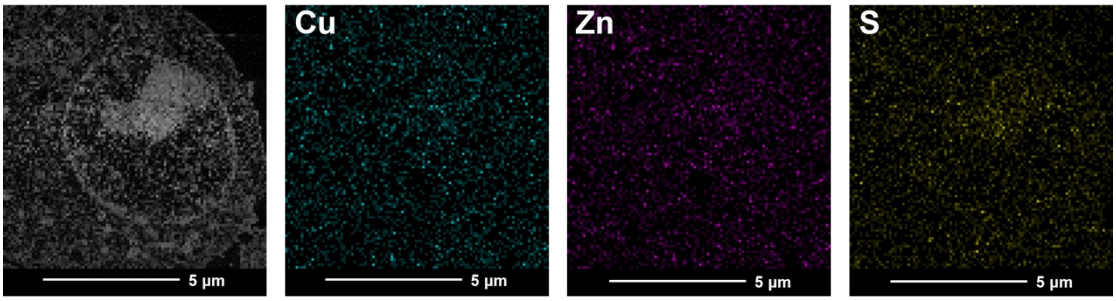

Figure S12. High-angle annular dark-field scanning transmission electron microscopy (HAADF-STEM) imaging and elemental mapping for 4T1 cells.

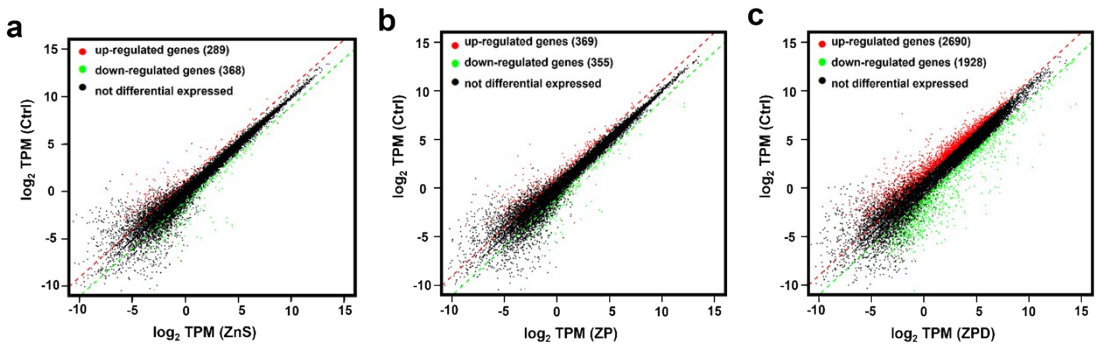

Figure S13. Transcripts per million (TPM) difference between different comparison. (a) ZnS vs Ctrl, (b) ZP vs Ctrl, and (c) ZPD vs Ctrl.

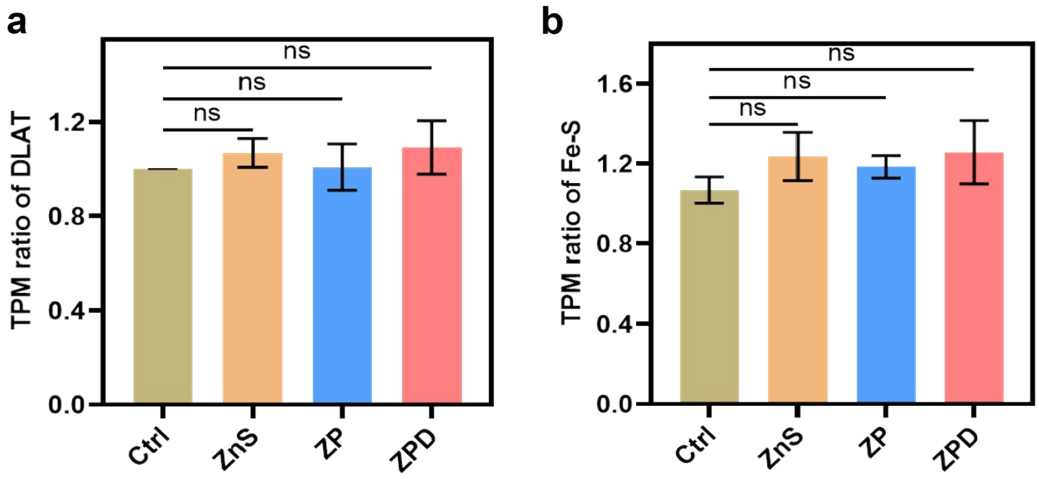

Figure S14. TPM ratio of different targeting proteins including dihydrolipoamide S-acetyltransferase (DLAT) (a) and Fe-S (iron-sulfur) clusters (b).

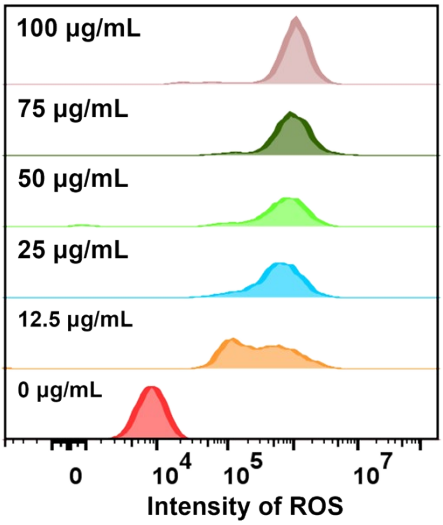

Figure S15. Cellular ROS by flow cytometry with different ZPD concentrations.

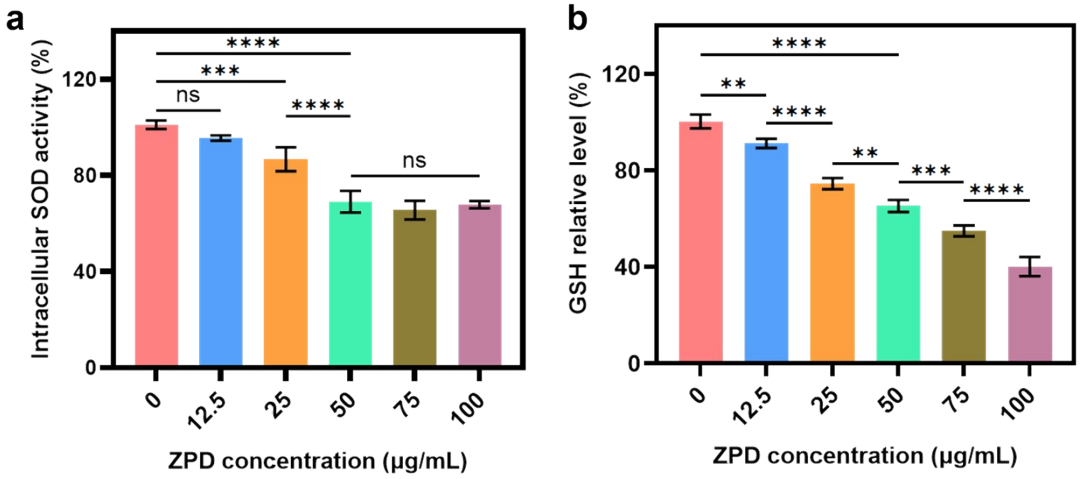

Figure S16. (a) Intracellular SOD deactivation by ZPD in 4T1 cells. (b) Change in GSH content by ZPD in 4T1 cells. Each error bar represents the standard deviation of four independent measurements. Ordinary one-way ANOVA was used for discrepancy analysis (*P<0.05, **P<0.01, ***P<0.001, ****P<0.0001).

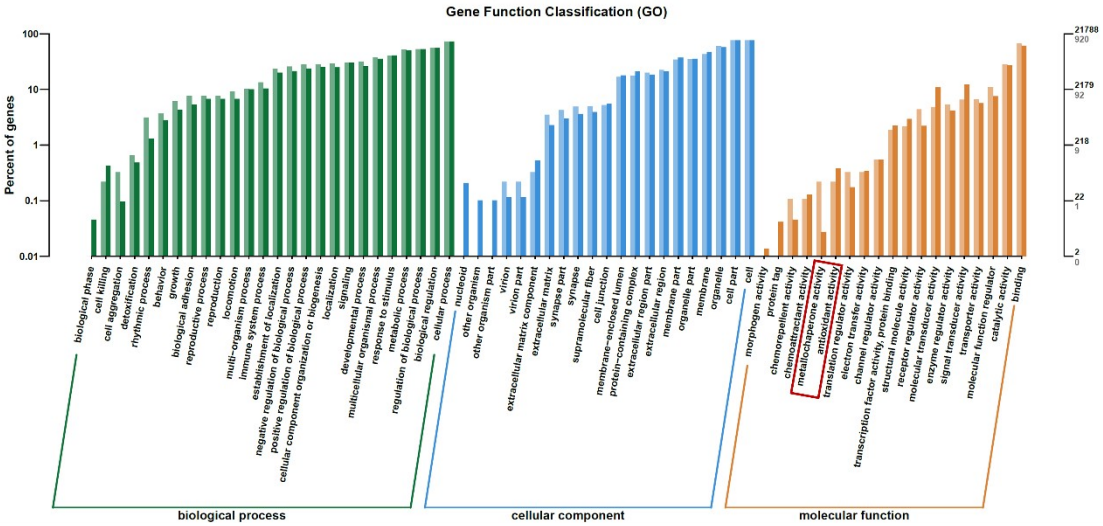

Figure S17. Gene function classification analysis of ZPD vs Ctrl.

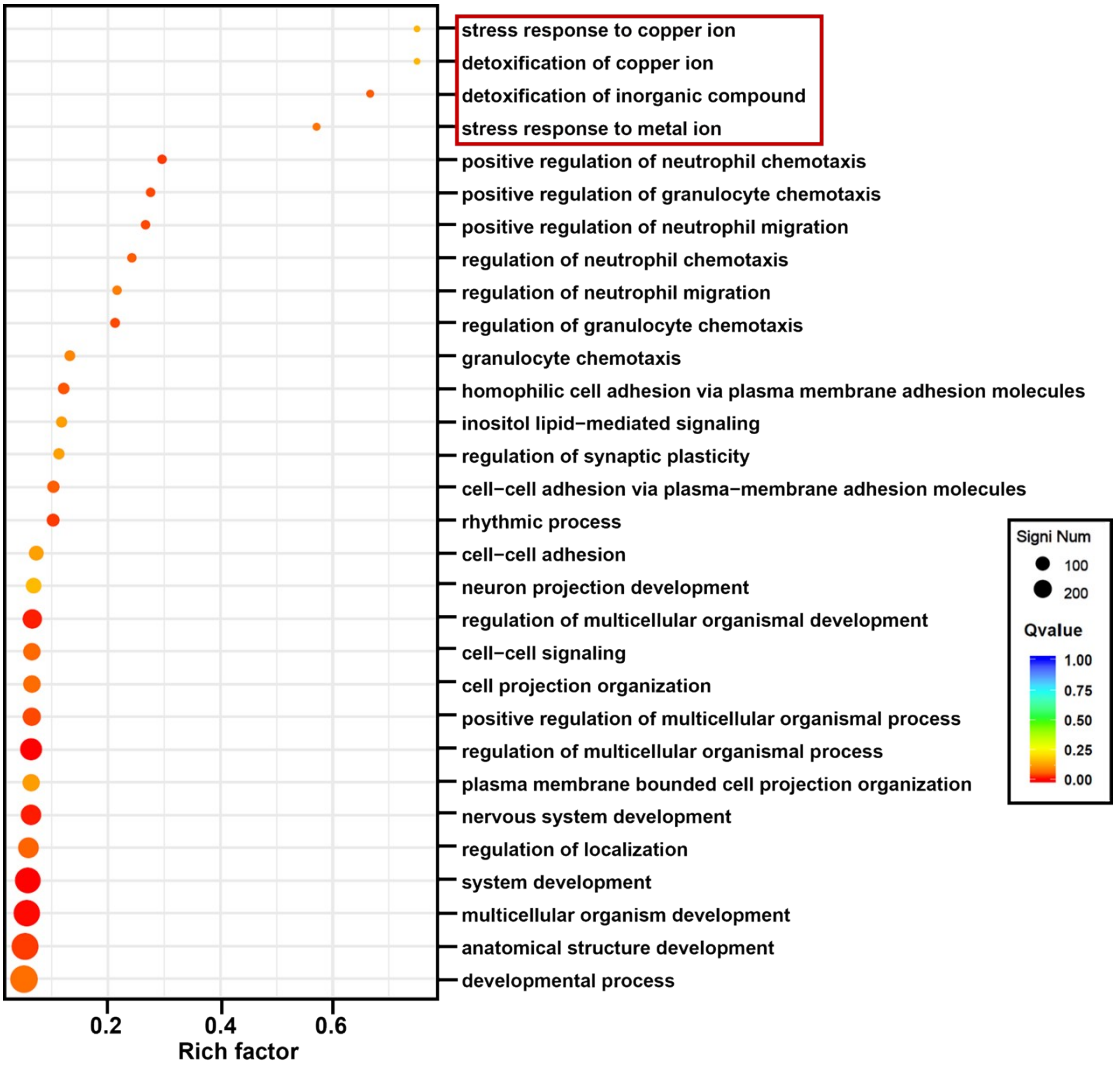

Figure S18. GO (gene ontology) enrichment analysis of ZPD vs Ctrl.

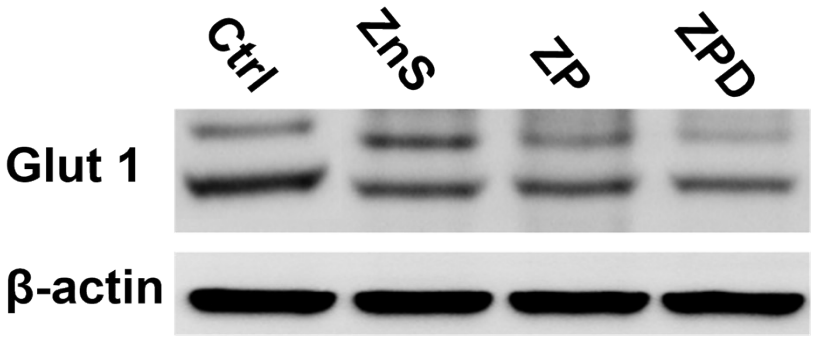

Figure S19. Analysis of Glut 1 expression by western blotting.

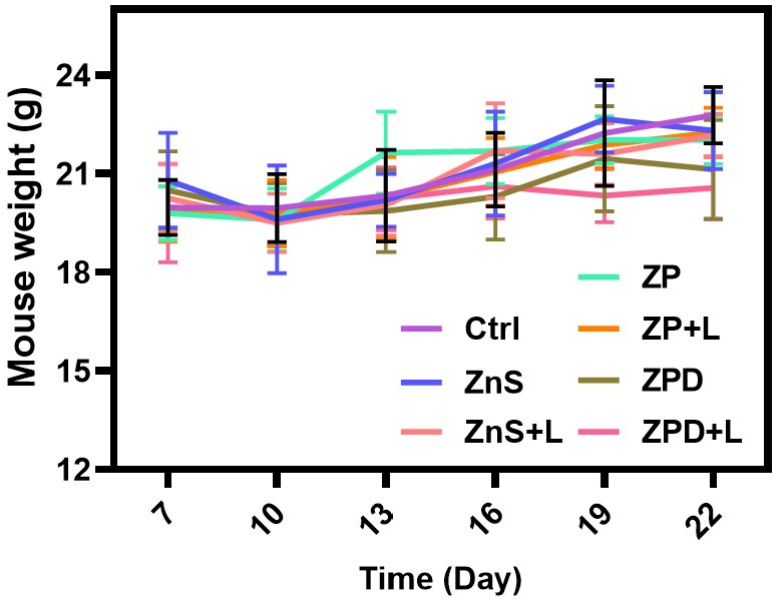

Figure S20. Changes in mouse weight after indicated treatments. Each error bar represents the standard deviation of four independent measurements.

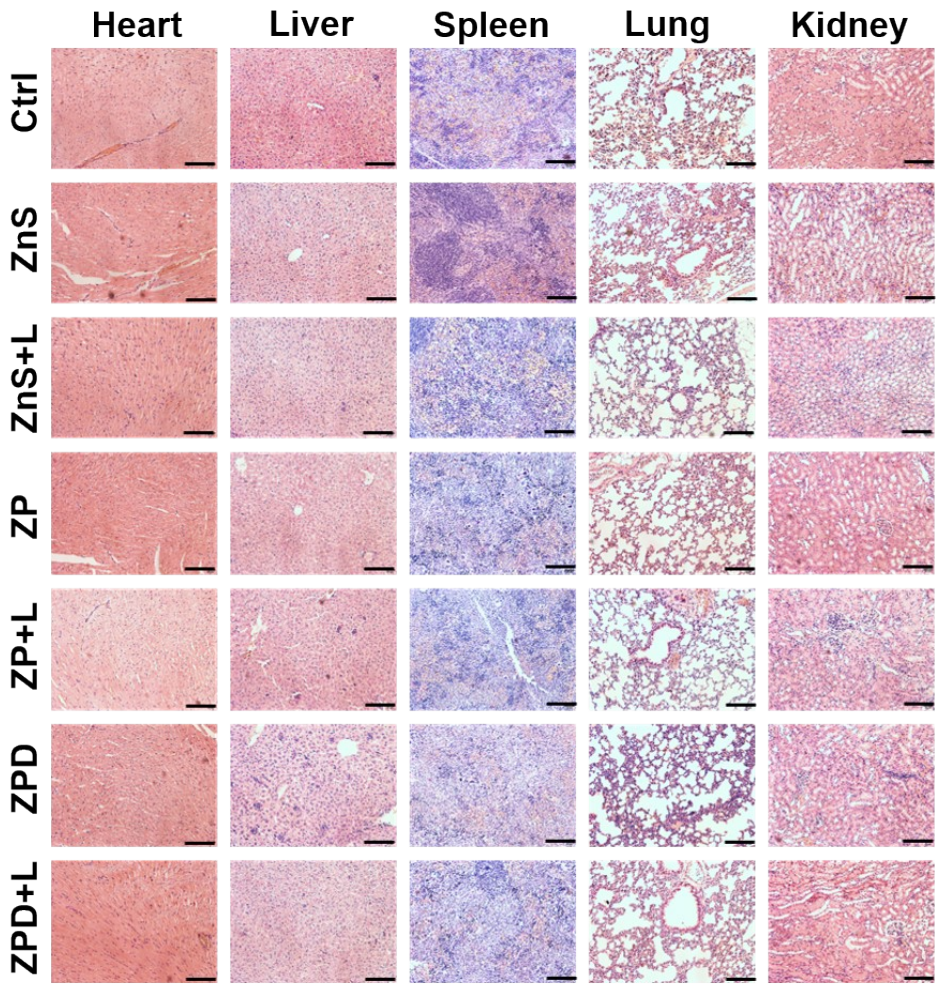

Figure S21. H&E staining of major organs after indicated treatments. Scale bar: 500 μm.

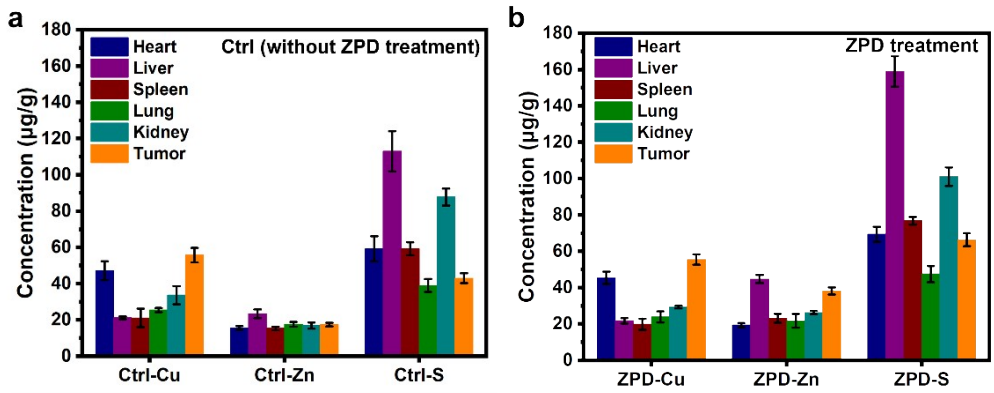

Figure S22. Biodistribution of Cu, Zn and S between Ctrl and ZPD-treated groups. Each error bar represents the standard deviation of three independent measurements.

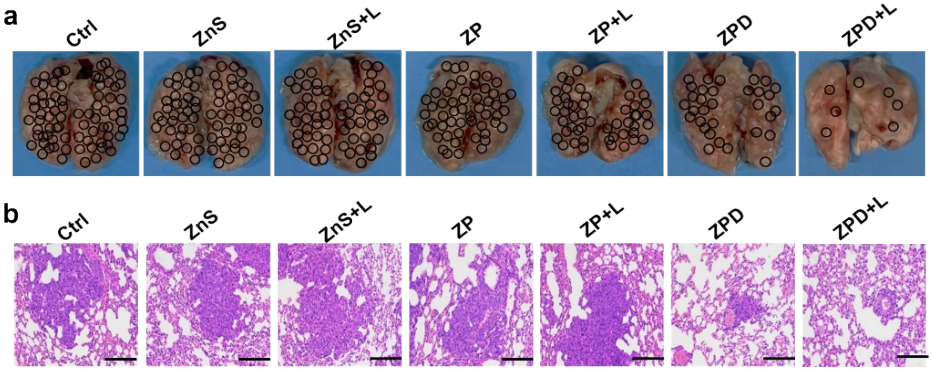

Figure S23. Anti-metastasis ability analysis. (a) Images of metastatic nodules. (b) H&E staining of metastatic nodules. Scale bar: 500 μm.

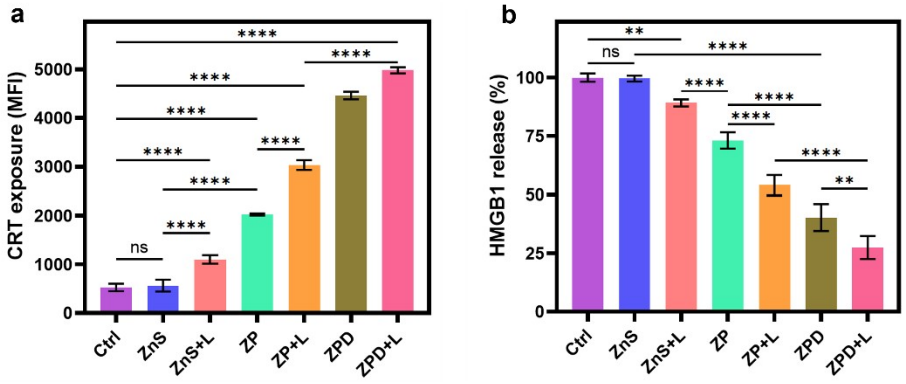

Figure S24. (a) Quantification of CRT exposure by fluorescent intensity. (b) HMGB1 release percentage after indicated treatments. Each error bar represents the standard deviation of four independent measurements. Ordinary one-way ANOVA was used for discrepancy analysis (*P<0.05, **P<0.01, P<0.001, ****P<0.0001).

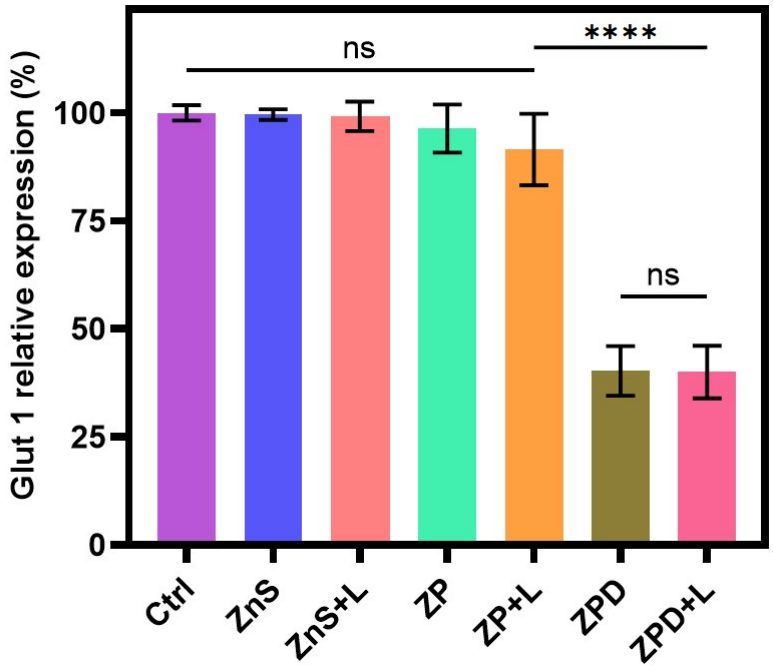

Figure S25. Decreasing percentage of Glut 1 relative expression after indicated treatments by fluorescent intensity measurement. Each error bar represents the standard deviation of four independent measurements. Ordinary one-way ANOVA was used for discrepancy analysis (*P<0.05, **P<0.01, P<0.001, ****P<0.0001).

References

[1] Ravitz, S. F. The solubilities and free energies of some eetallic sulfides. *The Journal of Physical Chemistry* **1936**, *40*, 61.

[2] Goates, J. R.; Gordon, M. B.; Faux, N. D. Calculated values for the aolubility product constants of the metallic sulfides. *Journal of the American Chemical Society* **1952**, *74*, 835.

[3] Waggoner, W. H. The solubility product constants of the metallic sulfides. *Journal of Chemical Education* **1958**, *35*, 339.

[4] Yu, J.; Zhang, J.; Liu, S. Ion-exchange synthesis and enhanced visible-light photoactivity of CuS/ZnS nanocomposite hollow spheres. *The Journal of Physical Chemistry C* **2010**, *114*, 13642.

[5] Zhang, J.; Yu, J.; Zhang, Y.; Li, Q.; Gong, J. R. J. N. l. Visible light photocatalytic H^2-production activity of CuS/ZnS porous nanosheets based on photoinduced interfacial charge transfer. *Nano Letters* **2011**, *11*, 4774.

[6] Mondal, C.; Singh, A.; Sahoo, R.; Sasmal, A. K.; Negishi, Y.; Pal, T. Preformed ZnS nanoflower prompted evolution of CuS/ZnS p–n heterojunctions for exceptional visible-light driven photocatalytic activity. *New Journal of Chemistry* **2015**, *39*, 5628.

[7] Zhao, X.; Zhao, K.; Su, J.; Sun, L. TiO2/CuS core-shell nanorod arrays with aging-induced photoelectric conversion enhancement effect. *Electrochemistry Communications* **2020**, *111*, 106648.

[8] Daskalakis, I.; Vamvasakis, I.; Papadas, I. T.; Tsatsos, S.; Choulis, S. A.; Kennou, S.; Armatas, G. S. Surface defect engineering of mesoporous Cu/ZnS nanocrystal-linked networks for improved visible-light photocatalytic hydrogen production. *Inorganic Chemistry Frontiers* **2020**, *7*, 4687.

[9] Bano, S.; Raj, S. I.; Khalilullah, A.; Jaiswal, A.; Uddin, I. Selective and sensitive cation exchange reactions in the aqueous starch capped ZnS nanoparticles with tunable composition, band gap and color for the detection and estimation of Pb2+, Cu2+ and Hg2+. *Journal of Photochemistry and Photobiology A: Chemistry* **2021**, *405*, 112925.

[10] Zhai, S.; Abraham, A. M.; Chen, B.; Fan, Z.; Hu, J.; Cai, Z.; Thangadurai, V. Abundant Canadian pine with polysulfide redox mediating ZnS/CuS nanocomposite to attain high-capacity lithium sulfur battery. *Carbon* **2022**, *195*, 253.

[11] Shetty, A.; Mishra, S. K.; De, A.; Chandra, S. Smart releasing CuS/ZnS nanocomposite dual drug carrier and photothermal agent for use as a theranostic tool for cancer therapy. *Journal of Drug Delivery Science and Technology* **2022**, *70*, 103252.

[12] Zhang, T.; Yan, B.; Zhang, L.; Yang, X. Ultrathin heterostructured ZnS/SnS2/CuS nanoflakes filled in N-doped carbon nanoboxes as novel cathode hosts for Li-SeS2 batteries. *Journal of Alloys and Compounds* **2024**, *990*, 174419.

[13] Mao, X.; Schimmer, A. D. The toxicology of Clioquinol. *Toxicology Letters* **2008**, *182*, 1.

[14] Chen, L.; Min, J.; Wang, F. Copper homeostasis and cuproptosis in health and disease. *Signal Transduction and Targeted Therapy* **2022**, *7*, 378.

[15] Huang, J.; Campian, J. L.; Gujar, A. D.; Tran, D. D.; Lockhart, A. C.; DeWees, T. A.; Tsien, C. I.; Kim, A. H. A phase I study to repurpose disulfiram in combination with temozolomide to treat newly diagnosed glioblastoma after chemoradiotherapy. *Journal of Neuro-Oncology* **2016**, *128*, 259.

[16] Shao, S.; Si, J.; Shen, Y. Copper as the Target for Anticancer Nanomedicine. *Advanced Therapeutics* **2019**, *2*, 1800147.

[17] Ford, E. S. Serum copper concentration and coronary heart disease among US adults. *American Journal of Epidemiology* **2000**, *151*, 1182.

[18] Walshe, J. M. Penicillamine, a new oral therapy for Wilson's disease. *The American Journal of*

Medicine **1956**, *21*, 487.
[19] Bandmann, O.; Weiss, K. H.; Kaler, S. G. Wilson's disease and other neurological copper disorders. *The Lancet Neurology* **2015**, *14*, 103.
[20] Brewer, G. J.; Dick, R. D.; Grover, D. K.; LeClaire, V.; Tseng, M.; Wicha, M.; Pienta, K.; Redman, B. G.; Jahan, T.; Sondak, V. K.; Strawderman, M.; LeCarpentier, G.; Merajver, S. D. Treatment of metastatic cancer with tetrathiomolybdate, an anticopper, antiangiogenic agent: Phase I study. *Clinical Cancer Research* **2000**, *6*, 1.
[21] Weiss, K. H.; Askari, F. K.; Czlonkowska, A.; Ferenci, P.; Bronstein, J. M.; Bega, D.; Ala, A.; Nicholl, D.; Flint, S.; Olsson, L.; Plitz, T.; Bjartmar, C.; Schilsky, M. L. Bis-choline tetrathiomolybdate in patients with Wilson's disease: an open-label, multicentre, phase 2 study. *The Lancet Gastroenterology & Hepatology* **2017**, *2*, 869.
[22] Wang, J.; Luo, C.; Shan, C.; You, Q.; Lu, J.; Elf, S.; Zhou, Y.; Wen, Y.; Vinkenborg, J. L.; Fan, J.; Kang, H.; Lin, R.; Han, D.; Xie, Y.; Karpus, J.; Chen, S.; Ouyang, S.; Luan, C.; Zhang, N.; Ding, H.; Merkx, M.; Liu, H.; Chen, J.; Jiang, H.; He, C. Inhibition of human copper trafficking by a small molecule significantly attenuates cancer cell proliferation. *Nature Chemistry* **2015**, *7*, 968.
[23] Shao, S.; Zhou, Q.; Si, J.; Tang, J.; Liu, X.; Wang, M.; Gao, J.; Wang, K.; Xu, R.; Shen, Y. A non-cytotoxic dendrimer with innate and potent anticancer and anti-metastatic activities. *Nature Biomedical Engineering* **2017**, *1*, 745.
[24] Cui, L.; Gouw, A. M.; LaGory, E. L.; Guo, S.; Attarwala, N.; Tang, Y.; Qi, J.; Chen, Y.-S.; Gao, Z.; Casey, K. M.; Bazhin, A. A.; Chen, M.; Hu, L.; Xie, J.; Fang, M.; Zhang, C.; Zhu, Q.; Wang, Z.; Giaccia, A. J.; Gambhir, S. S.; Zhu, W.; Felsher, D. W.; Pegram, M. D.; Goun, E. A.; Le, A.; Rao, J. Mitochondrial copper depletion suppresses triple-negative breast cancer in mice. *Nature Biotechnology* **2021**, *39*, 357.